

PAPER View Article Online



Cite this: Phys. Chem. Chem. Phys., 2019, 21, 19764

Received 5th July 2019, Accepted 15th August 2019

DOI: 10.1039/c9cp03786a

rsc.li/pccp

Superoctahedral two-dimensional metallic boron with peculiar magnetic properties†

Nikolay V. Tkachenko, Da Dmitriy Steglenko, Db Nikita Fedik, Db Natalia M. Boldyreva, BRUSIAN M. Minyaev, Db Vladimir I. Minkin Db and Alexander I. Boldyrev D**

Among the diversity of new materials, two-dimensional crystal structures have been attracting significant attention from the broad scientific community due to their promising applications in nanoscience. In this study we predict a novel two-dimensional ferromagnetic boron material, which has been exhaustively studied with DFT methods. The relaxed structure of the 2D-B₆ monolayer consists of slightly flattened octahedral units connected with 2c-2e B-B σ -bonds. The calculated phonon spectrum and *ab initio* molecular dynamics simulations reveal the thermal and dynamical stability of the designed material. The calculation of the mechanical properties indicate a relatively high Young's modulus of 149 N m⁻¹. Moreover, the electronic structure indicates the metallic nature of the 2D-B₆ sheets, whereas the magnetic moment per unit cell is found to be 1.59 $\mu_{\rm B}$. The magnetism in the 2D-B₆ monolayer can be described by the presence of two unpaired delocalized bonding elements inside every distorted octahedron. Interestingly, the nature of the magnetism does not lie in the presence of half-occupied atomic orbitals, as was shown for previously studied magnetic materials based on boron. We hope that our predictions will provide promising new ideas for the further fabrication of boron-based two-dimensional magnetic materials.

Introduction

The diversity of boron allotropes is fascinating. Containing one-dimensional, two-dimensional, and three-dimensional structures in its arsenal, boron is one of the most prospective elements for material science. A wide range of structures, such as nanowires, nanotubes, clusters, fullerenes, and 2D sheets, has been studied both theoretically and experimentally in recent years. Unique electronic properties, such as Dirac cones, were found for several 2D boron allotropes. An even hotter topic is the search for two-dimensional boron structures with magnetic properties due to their potential use in microelectronic and spintronic devices. Although the design of two-dimensional ferromagnetic materials is an extremely interesting and prospective topic, there are still few examples of theoretical 23-35 and experimental 36,37 reports. To the best of our knowledge, only

one 2D material made of boron with magnetic properties has been predicted to date.²⁰ However, it was shown that M-boron (a monolayer consisting of B20 polyhedrons) should be an antiferromagnetic material with ferromagnetic surface ordering. Following the idea of constructing 2D materials from polyhedrons, we decided to test a monolayer material constructed from boron octahedrons. Three-dimensional bulk materials with octahedral B₆ fragments were experimentally obtained previously. Their crystal structures always include a metal atom (Ca, La, etc.)38,39 because two electrons should be added to obtain a stable closo B₆ structure according to Wade's rules. 40,41 However, in the current work we predicted a stable superoctahedral magnetic boron material without the inclusion of any metal atoms. Therefore, this material is the second example of magnetic boron and the first example of ferromagnetic two-dimensional boron ever predicted.

Computational methods

All calculations for the solid state systems were performed using Vienna *Ab initio* Simulation Package⁴² (VASP) code with PAW^{43,44} pseudopotentials. The generalized gradient approximation (GGA) expressed by the PBE functional⁴⁵ was applied. For the structure relaxation, a large 700 eV energy cutoff with a

^a Department of Chemistry and Biochemistry, Utah State University, Logan, Utah 84322, USA. E-mail: a.i.boldyrev@usu.edu

b Institute of Physical and Organic Chemistry, Southern Federal University, 194/2 Stachka Ave., 344090, Rostov-on-Don, Russian Federation

 $[\]dagger$ Electronic supplementary information (ESI) available: Spin charge density distribution for FM 2D-B₆; calculated phonon dispersion and phonon density of states for NM 2D-B₆; final frames of each MD simulation test; structures and relative energies of the lowest energy B₄H₆ isomers; chemical bonding analysis of the B₆H₆²⁻, B₆H₄²⁻ and B₆H₄ species. See DOI: 10.1039/c9cp03786a

PCCP Paper

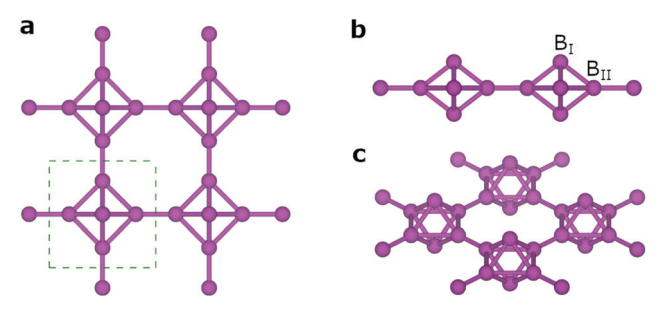


Fig. 1 (a) The top view of the 2D-B₆ structure. The unit cell is shown with a green dashed square. (b) The side view of the 2D-B₆ structure. The two different types of boron atoms are labeled B_I and B_{II}. (c) The angle view of the 2D-B₆ structure.

convergence threshold of 10⁻⁸ eV for the total energy was employed. The Brillouin zone was sampled by the Monkhorst-Pack method⁴⁶ with an automatic generated 31 \times 31 \times 5 Γ centered k-point grid. To eliminate the interaction between 2D-B₆ planes, the vacuum space was chosen to be 15 Å. The phonon dispersion was calculated *via* Phonopy code⁴⁷ using a $4 \times 4 \times 1$ supercell and a $7 \times 7 \times 1$ k-mesh. For more accurate calculation of the magnetism in the 2D-B₆ unit cell, the state-of-the-art hybrid functional of Heyd, Scuseria, and Ernzerhof (HSE06)48,49 was used. The energy cutoff for these calculations was set to 500 eV, the energy convergence criterion was set to 10^{-6} eV and a 17 \times 17×3 k-point grid was used. Band structure and DOS calculations for 2D-B₆ were performed at the PBE functional level with an 800 eV energy cutoff. To explore the magnetic ordering within the 2D-B₆ surface, optimization of the 2 \times 2 \times 1 supercell in nonmagnetic (NM), antiferromagnetic (AFM), and ferromagnetic (FM) configurations was performed.

To evaluate the thermal stability, ab initio Born-Oppenheimer molecular dynamics (BOMD) simulations for a $4 \times 4 \times 1$ supercell (96 atoms) were carried out. The time of the simulation was set to 5 ps with a time step of 1 fs. To calculate the molecular dynamics at 300 K, a longer time of 10 ps was set. Temperature control was performed using the Nosé-Hover method.50

The solid-state adaptive natural density partitioning (SSAdNDP)⁵¹ algorithm was used to analyze the bonding pattern of the 2D-B₆ structure. SSAdNDP follows an idea of the periodic NBO method⁵² and allowed us to obtain not only classical Lewis elements such as 1c-2e lone pairs and 2c-2e bonds but also delocalized bonding elements (nc-2e). A plane-wave calculation was performed using a 400 eV energy cutoff with a convergence threshold of 10^{-6} eV for the total energy and a k-point grid of $31 \times 31 \times 7$. Then, plane-wave density was projected into the cc-pVTZ⁵³ AO basis set. Previously, it was shown that the SSAdNDP is a powerful tool for analyzing chemical bonding in 2D materials. 54-65 All optimized geometries and obtained bonding patterns were visualized by Vesta software.66

The global minimum of a B₆H₄ cluster was found using the Coalescence Kick algorithm.⁶⁷ Five thousand trial structures were generated and optimized at the PBE0/3-21G level of theory^{68,69} for both singlet and triplet states. All structures within 20 kcal mol⁻¹ from global minimum (GM) were reoptimized at the PBE0/aug-cc-pVTZ level. The bonding pattern was obtained using the AdNDP algorithm⁷⁰ as implemented in the AdNDP 2.0 code. 71 All calculations for molecules were performed using the Gaussian16 program.⁷² All results of molecular calculations were visualized by ChemCraft 1.8 software.

Results and discussion

The optimized crystal structure of the 2D-B₆ monolayer belongs to the $P_{4/mmm}$ crystallographic group. The unit cell consists of six boron atoms ordered in a slightly flattened octahedron. For this type of symmetric structure, we can distinguish two types of equivalent boron atoms (Fig. 1b). The B_I-B_I, B_I-B_{II} and B_{II}-B_{II} lengths within the unit cell are 2.08 Å, 1.69 Å, and 1.89 Å, respectively. In turn, the B_{II}-B_{II} length between two neighboring unit cells is 1.62 Å, which is the shortest distance within the whole structure. The nature of these geometric features will be discussed below. For the magnetic properties, we found both nonmagnetic (NM) and ferromagnetic (FM) configurations of the unit cell. It is noteworthy to mention that the FM state is lower in energy than the NM state by 43 meV per atom; therefore, the former state represents the energetically more stable state of 2D-B₆. However, from the structural point of view, these two configurations almost coincide. For comparison, the lattice constants, total energies, and atomic positions are given in Table 1.

Because the magnetic properties of the designed material are our primary interest, we decided to study them at a more sophisticated level of theory. For a more accurate description of the magnetism, the HSE06 functional was used. The calculated magnetic moment per unit cell was found to be 1.59 $\mu_{\rm B}$. Notably, the magnetic moment is independent of the choice of density functional because almost the same results (1.56 $\mu_{\rm B}$) were obtained for the PBE functional. The spin charge distribution for the FM 2D-B₆ sheet shows that the spin density is

Table 1 Lattice constants, atomic positions and total energies of the NM and FM 2D-B₆ monolayers

Configuration	Туре	Atomic positions	a (Å)	b (Å)	c (Å)	$E_{\rm tot}$ (eV per atom)
FM	$egin{array}{c} B_{ m I} \ B_{ m II} \end{array}$	(0.5, 0.5, 0.569) (0.5, 0.5, 0.431) (0.189, 0.5, 0.5) (0.811, 0.5, 0.5) (0.5, 0.189, 0.5) (0.5, 0.811, 0.5)	4.292	4.292	14.999	-5.762
NM	$\begin{array}{c} B_{\rm I} \\ B_{\rm II} \end{array}$	(0.5, 0.5, 0.567) (0.5, 0.5, 0.433) (0.190, 0.5, 0.5) (0.810, 0.5, 0.5) (0.5, 0.190, 0.5) (0.5, 0.810, 0.5)	4.318	4.318	14.823	-5.719

FM AFM1 AFM2 NM E=0.00 eV E=0.10 eV E=0.10 eV E=1.02 eV

Fig. 2 Magnetic ordering and relative total energies for the $2 \times 2 \times 1$ supercell of the 2D-B₆ sheet.

localized not only on the top and bottom boron atoms of the B_6 octahedron but is delocalized through the structure (Fig. S1, ESI†). This type of delocalization may result in the partial 1.59 $\mu_{\rm B}$ magnetic moment per unit cell. To confirm the magnetic surface state, the 2 \times 2 \times 1 supercell of the 2D- B_6 sheet with different magnetic ordering was analyzed (Fig. 2). We found that the FM surface state is the most stable configuration; it is 0.10 and 1.02 eV per supercell lower in energy than the AFM and NM states, respectively. Therefore, 2D- B_6 is an exciting example of a ferromagnetic material with ferromagnetic surface ordering.

The dynamic stabilities of the FM and NM configurations of 2D- B_6 were tested by calculating their phonon dispersion curves and phonon densities of states. We showed that there are no low-lying dispersion curves entering the imaginary region in the whole Brillouin zone for the ferromagnetic configuration (Fig. 3). The highest optical mode corresponds to in-plane vibrations and reaches ≈ 40 THz (1334 cm $^{-1}$), indicating strong B–B interactions. Interestingly, only the ferromagnetic configuration is dynamically stable, while the nonmagnetic state has a large imaginary mode corresponding to the out-of-plane vibrations of $B_{\rm II}$ atoms (Fig. S2, ESI†).

In order to understand the electronic properties of the ferromagnetic 2D- B_6 material, we calculated its electronic band structure and density of states (Fig. 4). We found that both the spin up and spin down electrons have bands crossing the zero-energy level. As a result, 2D- B_6 has a nonzero density of states at the Fermi level. These facts prove that the 2D- B_6 sheet is metallic, without any band gap. For comparison, the previously predicted M-boron is an AFM semiconductor with an indirect band gap of 0.43 eV. 20

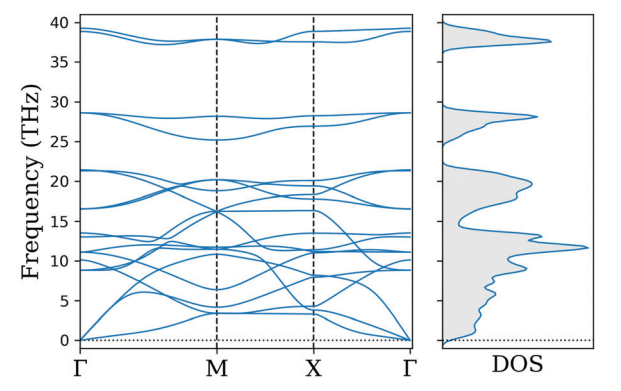


Fig. 3 Calculated phonon dispersion curves along the Γ -M-X- Γ path and phonon density of states for the ferromagnetic 2D-B₆ material.

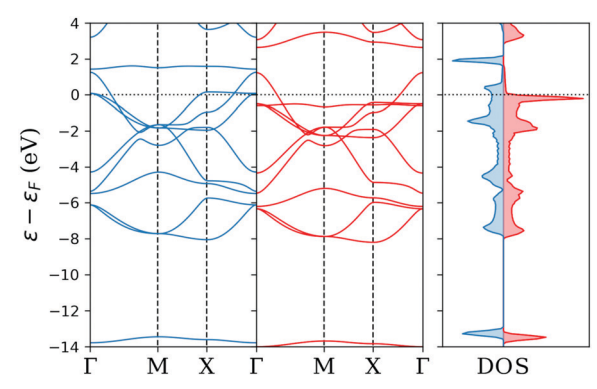


Fig. 4 Calculated electronic band structure along the Γ -M-X- Γ path and density of states for ferromagnetic 2D-B₆. The red curves correspond to the spin up electrons, while the spin down electrons are illustrated with blue curves. The Fermi level is shown as a horizontal dotted black line.

An essential property of a material suitable for practical applications is thermal stability. We performed spin-polarized ab initio Born-Oppenheimer molecular dynamics simulations at different temperatures (100 K, 300 K, and 450 K). The Nosé-Hover thermostat was used for temperature control. The time of the simulation was set to 5 ps with a time step of 1 fs. For the 300 K simulation, a longer time of 10 ps was chosen. A periodic $4 \times 4 \times 1$ supercell (96 atoms) was used; this cell size is large enough to demonstrate the structure and magnetic properties during the simulation. In Fig. 5, the fluctuations of the total magnetic moment and the temperature are shown as a function of the simulation time. The average total magnetic moment retains a remarkably large value at the end of the simulations $(25.4, 22.7 \text{ and } 16.7 \mu_B \text{ for } 100, 300, \text{ and } 450 \text{ K, respectively}).$ After 5 ps for the 100 K simulations and 10 ps for the 300 K simulations, we found no significant structure distortion (Fig. S3, ESI†). However, during the 450 K simulation, the structure was only stable for 3 ps. After that time, drastic structural deformations were observed. Thus, the 2D-B₆ structure is unstable at this high temperature; the octahedral fragments distorted severely and transformed into planar isomers, leading to a noticeable decrease in the magnetic moment of the material (Fig. 5). The root-mean square deviations from the 0 K bond lengths are 0.07, 0.14, and 4.61 Å for 100, 300 and 450 K, respectively. As a result of these calculations, we can declare that the ferromagnetic 2D-B₆ monolayer survives at temperatures up to 300 K, which opens a wide variety of potential applications. However, we should mention that this temperature does not correspond to the Curie temperature because the

PCCP Paper

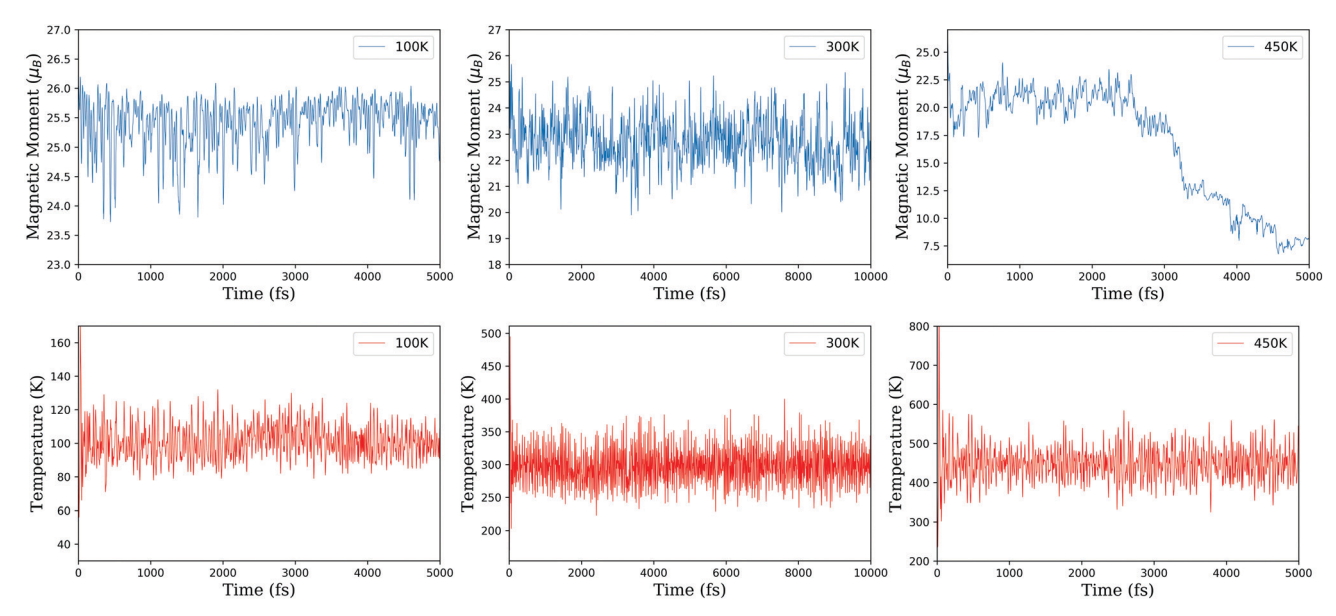


Fig. 5 Calculated fluctuations of the total magnetic moment and temperature vs. simulation time step at 100 K (left column), 300 K (center column) and 450 K (right column).

molecular dynamics simulation does not include spin dynamics. The obtained results indicate the stability of the magnetic state with respect to structural deformations.

Other important aspects of a promising material are its mechanical properties, which characterize the plasticity and elasticity of the material. The elastic constants, Young's modulus, and Poisson's ratio for the 2D-B6 monolayer are listed in Table 2 (only two elastic constants are presented because the structure is isotropic). The Young's modulus and Poisson's ratio were calculated according to the following formulas:

$$Y_{\rm 2D} = \frac{c_{11}^2 - c_{12}^2}{c_{11}} \tag{1}$$

$$\nu = \frac{c_{12}}{c_{11}} \tag{2}$$

The question of how to synthesize this material remains open for the moment. However, we hope that we are currently on the right track. Thus, studies on the preparation of singly charged compounds containing an octahedral B₆ fragment are underway.⁷³ We believe that the results of this research will be helpful for the synthesis of 2D-B₆.

To obtain insight into the chemical bonding of the 2D-B₆ monolayer, we firstly decided to analyze the bonding pattern for a model D_{4h}-symmetric B₆H₄ cluster. For the spin state of the model cluster, we chose a triplet as the closest approximation to our ferromagnetic sheet. We should mention that the investigated structure has one imaginary frequency because it

Table 2 The calculated elastic constants (c_{ij} , in N m⁻¹), Young's modulus $(Y_{2D}, \text{ in N m}^{-1})$, and Poisson's ratio (ν) of the 2D-B₆ monolayer

Structure	c_{11}	c_{12}	c ₆₆	Y_{2D}	ν
2D-B ₆	150.06	-12.59	9.84	149.01	-0.08

was forced to belong to the D_{4h} symmetry group. The gradient descending along the imaginary frequency led us to the less symmetric C_s structure. However, this distortion is not significant for the exploration of chemical bonding, and in the subsequent discussion, the more symmetric structure will be considered for convenience. The analysis of the potential energy surface via the coalescence kick algorithm reveals that

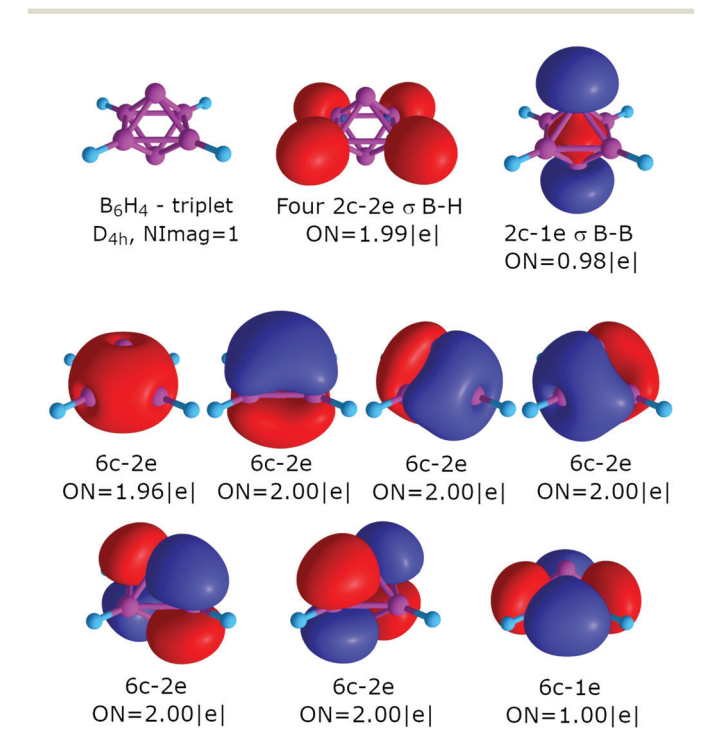


Fig. 6 Overall chemical bonding picture obtained for the B₆H₄ cluster in the triplet state. The abbreviation ON denotes the occupation number of a certain bond.

cluster will be discussed.

the distorted octahedral geometry of B_6H_4 is 5.9 kcal mol^{-1} higher in energy than the planar global minimum structure (Fig. S6, ESI†). However, the considered structure is still one of the lowest energy isomers for the chosen stoichiometry. In the gas phase, singlet state GM is more favorable than triplet GM by 9.3 kcal mol^{-1} . For the octahedral structures as building blocks for the 2D- B_6 monolayer, the singlet structure is lower in energy by only 1.4 kcal mol^{-1} . Obviously, in the crystal environment, the triplet state is stabilized because the calculated magnetic moment of the unit cell clearly indicates the presence of unpaired electrons; therefore, the bonding pattern for the triplet molecular

The results of the AdNDP analysis are presented in Fig. 6. The bonding pattern can be described as four classical two-centered two-electron (2c-2e) B–H σ -bonds with an occupation number (ON) of 1.99 |e|, six 6c-2e bonds with ON = 2.00 to 1.96 |e|, and two unpaired alpha electrons which form a 2c-1e B–B bond with ON = 0.98 |e| and a 6c-1e bond with ON = 1.00 |e|. Unprecedently, the 1e bonds are perpendicular to each other; we have never observed this bonding feature before.

Because it is not quite an intuitive result, we decided to build an evolution path of the chemical bonding picture from the well-known $B_6H_6^{2-}$ cluster to the B_6H_4 species. The results can be found in the ESI.† The obtained bonding patterns for

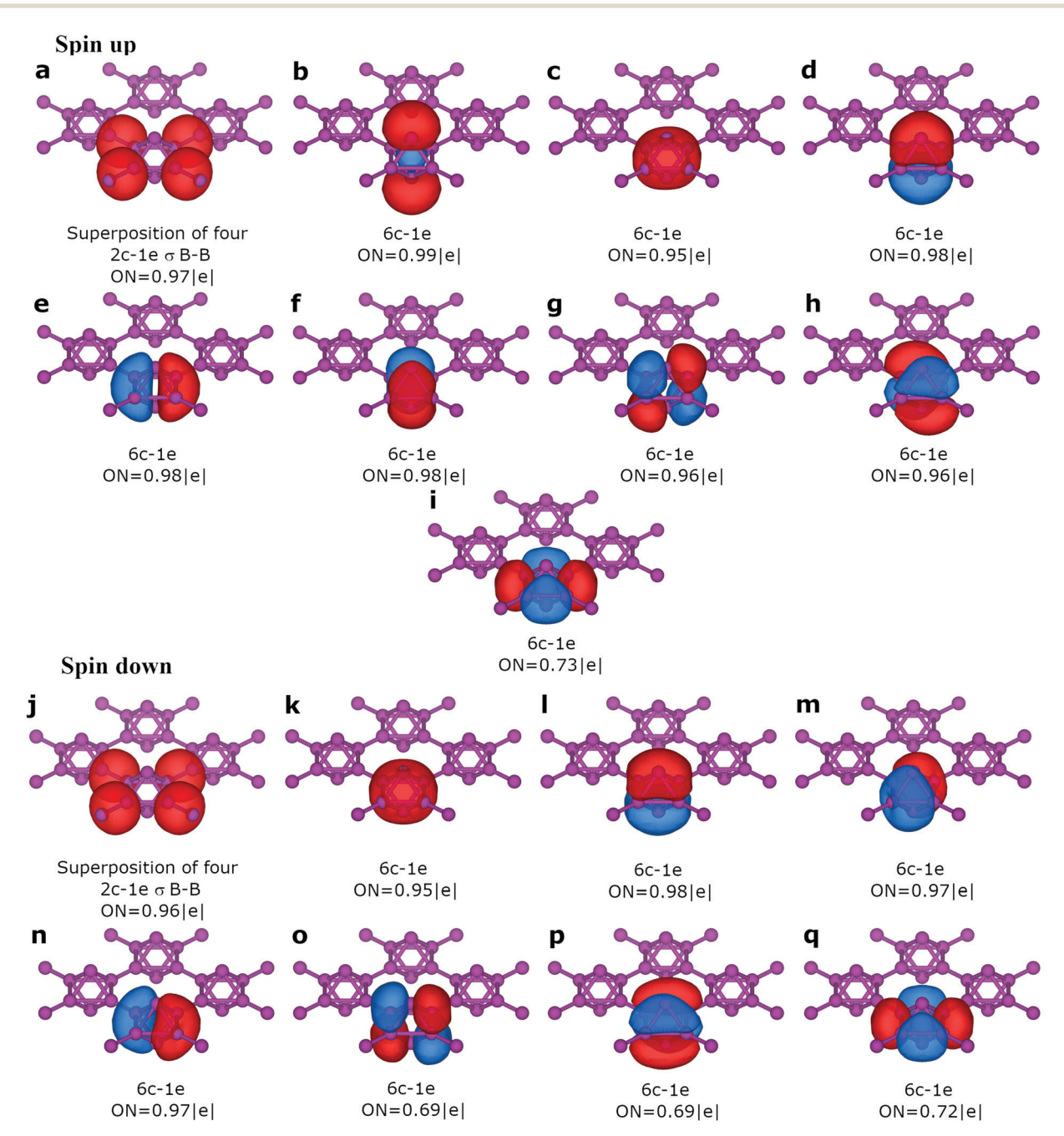


Fig. 7 Overall chemical bonding picture obtained for the 2D-B₆ sheet. The results for the spin up and spin down electrons are presented separately.

Paper

 $B_6H_6^{2-}$ and $B_6H_4^{2-}$ as well as the comparison of MO energies pushed us to the conclusion that the presented bonding pattern is correct (Fig. S7–S10, ESI†). It is worth noting that we expected to find two 1c-1e bonds at the top and bottom apexes of the B_6 unit (as was observed for the previously predicted M-boron²⁰). However, during the structure relaxation, we observed a change in the energy of the molecular orbitals which led to the formation of two one-electron bonds perpendicular to each other. These bonds provide a slightly flattened geometry for this cluster. We will see below that similar one-electron bonds were also found in the 2D- B_6 monolayer. These bonding elements are responsible for the ferromagnetic properties of this material.

To determine the bonding picture in 2D-B₆, we used the Solid State Adaptive Natural Density Partitioning (SSAdNDP) algorithm. Following the ideas extracted from the bonding of the B₆H₄ cluster, we obtained a very cognate bonding pattern for the solid state. The results of the SSAdNDP analysis for the spin up and spin down electrons are presented in Fig. 7. Each unit cell is bound with neighboring cells through classical 2c-2e B-B σ -bonds with ON = 1.93 |e| (the equivalent of B-H σ -bonds for the cluster). The remaining electrons form eight delocalized six-centered one-electron bonds, which are responsible for the binding interactions inside each flattened octahedron. For the spin up electrons, we found a 6c-1e bond with ON = 0.99 |e|(Fig. 7b) with a shape similar to the 2c-1e bond found in the B₆H₄ cluster. Indeed, the contributions of the two B_I atoms to the six-centered bond were found to be 97%. Therefore, we can consider it as a pure 2c-1e bond. This chemical bond can cause flattening of the B₆ octahedron. However, although the chemical bonding of the cluster and solid state coincide for several bonding elements, we noted that the last three 6c-1e bonds of the spin down electrons (Fig. 70-q) behave differently. Instead of having one electron on each of the two 6c bonds (Fig. 70 and p), as is observed in the case of B₆H₄, we have almost equal low filling of three 6c bonds. The sum of the occupancies gives us about 2 electrons. This interesting behavior may be associated with more explicit degeneration of these orbitals in the case of the solid state. Despite the described discrepancies in bonding patterns, the calculation of the difference between the spin up and spin down occupancies provides us with a value of 1.58 |e|, which is in very good agreement with the calculated magnetic moment per unit cell (1.59 $\mu_{\rm B}$).

Conclusions

To summarize, we designed and computationally tested a novel ferromagnetic superoctahedral 2D boron material. Based on the phonon spectrum and molecular dynamics simulations, we managed to show that the 2D-B₆ monolayer is dynamically and thermally stable. Moreover, it has substantial magnetic properties, and the calculated magnetic moment per unit cell was found to be 1.59 $\mu_{\rm B}$. The electronic structure indicates that this material is metallic, and its bonding pattern consists of classical 2c-2e bonds between unit cells; the chemical bonding inside of

the unit cell almost completely consists of six-centered bonds, which are responsible for the magnetic properties. To the best of our knowledge, the material designed in our work is the second example of a magnetic 2D sheet and the first example of a ferromagnetic metallic 2D sheet formed from pure boron. Therefore, we believe that this material is of great interest to modern material science, and its thermal and mechanical stabilities promise a wide range of applications once it is experimentally obtained.

Author contributions

The manuscript was written through contributions of all authors. All authors have given approval to the final version of the manuscript.

Conflicts of interest

The authors declare no competing financial interest.

Acknowledgements

The work was supported by the USA National Science Foundation (Grant CHE-1664379) to A. I. B.; D. S., R. M. M., V. I. M. and A. I. B. thank the Russian Ministry of Science and Education for financial support (Agreement No. 14.Y26.31.0016).

References

- B. Albert and H. Hillebrecht, Angew. Chem., Int. Ed., 2009, 48, 8640.
- 2 A. P. Sergeeva, I. A. Popov, Z. A. Piazza, W. L. Li, C. Romanescu, L. S. Wang and A. I. Boldyrev, *Acc. Chem. Res.*, 2014, 474, 1349.
- 3 H. J. Zhai, B. Kiran, J. Li and L. S. Wang, *Nat. Mater.*, 2003, 2, 827.
- 4 N. Gonzalez Szwacki, A. Sadrzadeh and B. I. Yakobson, *Phys. Rev. Lett.*, 2007, **98**, 166804.
- 5 H. Tang and S. Ismail-Beigi, Phys. Rev. Lett., 2007, 99, 115501.
- 6 D. L. V. K. Prasad and E. D. Jemmis, *Phys. Rev. Lett.*, 2008, 100, 165504.
- 7 H. Tang and S. Ismail-Beigi, *Phys. Rev. B: Condens. Matter Mater. Phys.*, 2009, **80**, 134113.
- 8 S. Saxena and T. A. Tyson, *Phys. Rev. Lett.*, 2010, **104**, 245502.
- 9 M. Liu, V. I. Artyukhov and B. I. Yakobson, J. Am. Chem. Soc., 2017, 1395, 2111.
- 10 S. De, A. Willand, M. Amsler, P. Pochet, L. Genovese and S. Goedecker, *Phys. Rev. Lett.*, 2011, 106, 225502.
- 11 F. Liu, C. Shen, Z. Su, X. Ding, S. Deng, J. Chen, N. Xu and H. Gao, *J. Mater. Chem.*, 2010, **20**, 2197.
- 12 E. S. Penev, S. Bhowmick, A. Sadrzadeh and B. I. Yakobson, *Nano Lett.*, 2012, **12**, 2441.
- 13 X. Wu, J. Dai, Y. Zhao, Z. Zhuo, J. Yang and X. C. Zeng, *ACS Nano*, 2012, **6**, 7443.

- 14 D. V. Steglenko, S. A. Zaytsev, R. M. Minyaev and V. I. Minkin, *Neorg. Khim.*, 2019, **64**, 1.
- 15 H. Liu, J. Gao and J. Zhao, Sci. Rep., 2013, 3, 3238.
- 16 X. F. Zhou, X. Dong, A. R. Oganov, Q. Zhu, Y. Tian and H. T. Wang, *Phys. Rev. Lett.*, 2014, **112**, 085502.
- 17 X. F. Zhou, A. R. Oganov, X. Shao, Q. Zhu and H. T. Wang, Phys. Rev. Lett., 2014, 113, 176101.
- 18 H. J. Zhai, Y. F. Zhao, W. L. Li, Q. Chen, H. Bai, H. S. Hu, Z. A. Piazza, W. J. Tian, H. G. Lu, Y. B. Wu, Y. W. Mu, G. F. Wei, Z. P. Liu, J. Li, S. D. Li and L. S. Wang, *Nat. Chem.*, 2014, 6, 727.
- 19 M. Martinez-Canales, T. R. Galeev, A. I. Boldyrev and C. J. Pickard, *Phys. Rev. B*, 2017, **96**, 195442.
- 20 X. F. Zhou, A. R. Oganov, Z. Wang, I. A. Popov, A. I. Boldyrev and H. T. Wang, *Phys. Rev. B*, 2016, **93**, 085406.
- 21 Z. Zhang, E. S. Penev and B. I. Yakobson, *Chem. Soc. Rev.*, 2017, **46**, 6746.
- 22 Z. Zhang, Y. Yang, E. S. Penev and B. I. Yakobson, *Adv. Funct. Mater.*, 2017, 27, 1605059.
- 23 J. Zhou and Q. Sun, J. Am. Chem. Soc., 2011, 133, 15113.
- 24 Y. Liu, S. Bhowmick and B. I. Yakobson, *Nano Lett.*, 2011, 11, 3113.
- 25 Y. Ma, Y. Dai, M. Guo, C. Niu, Y. Zhu and B. Huang, *ACS Nano*, 2012, **6**, 1695.
- 26 A. Du, S. Sanvito and S. C. Smith, Phys. Rev. Lett., 2012, 108, 197207.
- 27 Z. Zhang, X. Zou, V. H. Crespi and B. I. Yakobson, *ACS Nano*, 2013, 7, 10475.
- 28 X. Li, X. Wu and J. Yang, J. Am. Chem. Soc., 2014, 136, 11065.
- 29 F. Wu, C. Huang, H. Wu, C. Lee, K. Deng and E. Kan, *Nano Lett.*, 2015, 15, 8277.
- 30 Y. Wang, S. S. Wang, Y. Lu, J. Jiang and S. A. Yang, *Nano Lett.*, 2016, **16**, 4576.
- 31 N. Miao, B. Xu, N. C. Bristowe, J. Zhou and Z. Sun, *J. Am. Chem. Soc.*, 2017, **139**, 11125.
- 32 H. Kumar, N. C. Frey, L. Dong, B. Anasori, Y. Gogotsi and V. B. Shenoy, *ACS Nano*, 2017, 11, 7648.
- 33 Y. Sun, Z. Zhuo, X. Wu and J. Yang, *Nano Lett.*, 2017, 17, 2771.
- 34 Y. Zhao, J. J. Zhang, S. Yuan and Z. Chen, *Adv. Funct. Mater.*, 2019, **29**, 1901420.
- 35 X. Zhou, X. Sun, Z. Zhang and W. Guo, *J. Mater. Chem. C*, 2018, **6**, 9675.
- 36 C. Gong, L. Li, Z. Li, H. Ji, A. Stern, Y. Xia, T. Cao, W. Bao, C. Wang, Y. Wang, Z. Qiu, R. Cava, S. G. Louie, J. Xia and X. Zhang, *Nature*, 2017, 546, 265.
- 37 B. Huang, G. Clark, E. Navarro-Moratalla, D. R. Klein, R. Cheng, K. L. Seyler, D. Zhong, E. Schmidgall, M. A. McGuire, D. H. Cobden, W. Yao, D. Xiao, P. Jarillo-Herrero and X. Xu, *Nature*, 2017, 546, 270.
- 38 J. Akimitsu, K. Takenawa, K. Suzuki, H. Harima and Y. Kuramoto, *Science*, 2001, 293, 1125.
- 39 P. H. Schmidt, D. C. Joy, L. D. Longinotti, H. J. Leamy, S. D. Ferris and Z. Fisk, *Appl. Phys. Lett.*, 1976, **29**, 400.
- 40 K. Wade, Chem. Commun., 1971, 792.
- 41 K. Wade, Adv. Inorg. Chem. Radiochem., 1976, 18, 1.

- 42 G. Kresse and J. Hafner, *Phys. Rev. B: Condens. Matter Mater. Phys.*, 1993, 47, 558.
- 43 P. E. Blöchl, Phys. Rev. B: Condens. Matter Mater. Phys., 1994, 50, 17953.
- 44 G. Kresse and D. Joubert, Phys. Rev. B: Condens. Matter Mater. Phys., 1999, 59, 1758.
- 45 J. P. Perdew, K. Burke and M. Ernzerhof, *Phys. Rev. Lett.*, 1996, 77, 3865.
- 46 H. J. Monkhorst and J. D. Pack, *Phys. Rev. B: Solid State*, 1976, **13**, 5188.
- 47 A. Togo, F. Oba and I. Tanaka, *Phys. Rev. B: Condens. Matter Mater. Phys.*, 2008, 78, 134106.
- 48 J. Heyd, G. E. Scuseria and M. Ernzerhof, *J. Chem. Phys.*, 2003, **118**, 8207.
- 49 J. Heyd, G. E. Scuseria and M. Ernzerhof, *J. Chem. Phys.*, 2006, **124**, 219906.
- 50 G. J. Martyna, M. L. Klein and M. Tuckerman, J. Chem. Phys., 1992, 97, 2635.
- 51 T. R. Galeev, B. D. Dunnington, J. R. Schmidt and A. I. Boldyrev, *Phys. Chem. Chem. Phys.*, 2013, **15**, 5022.
- 52 B. D. Dunnington and J. R. Schmidt, J. Chem. Theory Comput., 2012, 8, 1902.
- 53 T. H. Dunning, J. Chem. Phys., 1989, 90, 1007.
- 54 A. S. Ivanov, E. Miller, A. I. Boldyrev, Y. Kameoka, T. Sato and K. Tanaka, *J. Phys. Chem. C*, 2015, **119**, 12008.
- 55 H. Zhang, Y. Li, J. Hou, A. Du and Z. Chen, *Nano Lett.*, 2016, 16, 6124.
- 56 Z. H. Cui, E. Jimenez-Izal and A. N. Alexandrova, *J. Phys. Chem. Lett.*, 2017, **8**, 1224.
- 57 C. Pu, D. Zhou, Y. Li, H. Liu, Z. Chen, Y. Wang and Y. Ma, J. Phys. Chem. C, 2017, 121, 2669.
- 58 Y. Wang, M. Qiao, Y. Li and Z. Chen, *Nanoscale Horiz.*, 2018, 3, 327.
- 59 I. A. Popov and A. I. Boldyrev, *J. Phys. Chem. C*, 2012, **116**, 3147.
- 60 X. F. Zhou, A. R. Oganov, Z. Wang, I. A. Popov, A. I. Boldyrev and H. T. Wang, *Phys. Rev. B*, 2016, 93, 085406.
- 61 I. A. Popov, K. V. Bozhenko and A. I. Boldyrev, *Nano Res.*, 2012, 5, 117.
- 62 M. Martinez-Canales, T. R. Galeev, A. I. Boldyrev and C. J. Pickard, *Phys. Rev. B*, 2017, **96**, 195442.
- 63 L. M. Yang, I. A. Popov, A. I. Boldyrev, T. Heine, T. Frauenheim and E. Ganz, *Phys. Chem. Chem. Phys.*, 2015, 17, 17545.
- 64 L. M. Yang, I. A. Popov, T. Frauenheim, A. I. Boldyrev, T. Heine, V. Bačić and E. Ganz, *Phys. Chem. Chem. Phys.*, 2015, 17, 26043.
- 65 L. M. Yang, V. Bačić, I. A. Popov, A. I. Boldyrev, T. Heine, T. Frauenheim and E. Ganz, J. Am. Chem. Soc., 2015, 137, 2757.
- 66 K. Momma and F. Izumi, J. Appl. Crystallogr., 2011, 44, 1272.
- 67 A. P. Sergeeva, B. B. Averkiev, H. J. Zhai, A. I. Boldyrev and L. S. Wang, *J. Chem. Phys.*, 2011, **134**, 224304.
- 68 C. Adamo and V. Barone, J. Chem. Phys., 1999, 110, 6158.
- 69 J. S. Binkley, J. A. People and W. J. Hehre, *J. Am. Chem. Soc.*, 1980, **102**, 939.
- 70 D. Y. Zubarev and A. I. Boldyrev, *Phys. Chem. Chem. Phys.*, 2008, **10**, 5207.

- 71 N. V. Tkachenko and A. I. Boldyrev, *Phys. Chem. Chem. Phys.*, 2019, **21**, 9590.
- 72 M. J. Frisch, et al., Gaussian 16, Revision B.01, Gaussian, Inc., 2016.
- 73 X. Mu, J. C. Axtell, N. Bernier, K. Kirlikovali, D. Jung, A. Umanzor, K. Qian, X. Chen, K. Bay, M. Kirollos, A. L. Rheingold, K. N. Houk and A. Spokoyny, Preprint at ChemRxiv, 2019, DOI: 10.26434/chemrxiv.8097542.v1.